Toward the Optimized Spintronic Response of Sn-Doped IrO$_2$ Thin Films

Eduardo Arias-Egido,* María Angeles Laguna-Marco, Cristina Piquer, Roberto Boada, and Sofía Díaz-Moreno

Amorphous and polycrystalline Sn-doped IrO$_2$ thin films, Ir$_{1-x}$Sn$_x$O$_2$, are grown for the first time. Their electrical response and strength of the spin–orbit coupling are studied in order to better understand and tailor its performance as spin current detector material. These experiments prove that the resistivity of IrO$_2$ can be tuned over several orders of magnitude by controlling the doping content in both the amorphous and the polycrystal-line state. In addition, growing amorphous samples increase the resistivity, thus improving the spin current to charge current conversion. As far as the spin–orbit coupling is concerned, the system not only remains in a strong spin–orbit coupling regime but it seems to undergo a slight enhancement in the amorphous state as well as in the Sn-doped samples.

1. Introduction

In the quest for new materials in the field of spintronics, those with significant spin-orbit coupling (SOC) are generating increasing interest. The strong SOC makes it possible to effi-ciently convert charge-currents on pure spin currents and vice versa via the so-called spin Hall effect (SHE) and inverse spin Hall effect (ISHE), respectively.[1–3] Among the explored mate-rials, IrO$_2$ has been suggested as the most promising for spin detection.[4] Interestingly enough, according to the work by Fuji-wara et al.,[4] the performance of IrO$_2$ as spin detector would be even better in the amorphous state. This is quite a puzzling

E. Arias-Egido, Dr. M. A. Laguna-Marco,
Dr. C. Piquer Instituto de Ciencia de
Materiales de Aragón
CSIC – Universidad de Zaragoza
Zaragoza 50009, Spain
E-mail: earias@unizar.es
E. Arias-Egido, Dr. M. A. Laguna-Marco,
Dr. C. Piquer Departamento de Física de la
Materia Condensada Universidad de Zaragoza
Zaragoza 50009, Spain

Dr. R. Boada
Department of Chemistry
Universitat Autònoma de
Barcelona 08193 Bellaterra,
Barcelona, Spain
Dr. R. Boada, Dr. S. Díaz-Moreno
Diamond Light Source Ltd
Harwell Science and Innovation
Campus Didcot, Oxfordshire OX11
0DE, UK

result, as the formation of cleaner and better-defined interfaces, and therefore superior diffusion process through the interface between IrO$_2$ layer and the spin-transport layer, is expected in the polycrys-talline state. Understanding the origin of this surprising behavior may be the key to find optimized spintronic materials. How-ever, no explanation has been proposed so far.

From a practical point of view, the ideal spin detector should have high electrical resistivity, ρ_C, and a large spin Hall angle, α_{SH}, since the electric voltage, ΔV_{ISHE}, generated by a spin current, I_S, is directly proportional to both: $\Delta V_{ISHE} = \alpha_{SH}\rho_C I_S$.[5,6] The large α_{SH}, owed to the strong SOC, is typically found in heavy transition metals. However, such materials typi-cally present very low electrical resistivity. Although in IrO$_2$ the resistivity is relatively high, it still belongs to the family of electrically conductive transition metal oxides, with $\rho_C \approx 10^2$ µΩ cm.[4,7–10] Therefore, in order to improve the usability of IrO$_2$ as spin detector, it is necessary to increase its resistivity without compromising other properties, especially its high SOC.

One possible way to do so is by introducing doping elements as "impurities" acting as barriers for the conductive electrons. This is expected not only to increase the resistivity but also the α_{SH} through an extrinsic spin Hall effect.[11–13] Choosing Sn as the dopant element is especially interesting. SnO$_2$ presents an insulating behavior and, like IrO$_2$, grows in the rutile structure. The only difference is an increase in the volume cell ≈10%. This will presumably make it easier for Sn to occupy Ir sites without any drastic structural change. Moreover, Sn^{4+} doping will not modify the electronic configuration of Ir, which will remain as Ir^{4+} irrespective of the doping content.

The present work aims to improve our understanding of the spintronic response of IrO$_2$, as well as finding effective ways to optimize it. To this end, Sn-doped IrO$_2$ thin films with different doping content and microstructure, i.e., amorphous and poly-crystalline, have been explored.

2. Results and Discussion

Thin films of ≈100 nm were fabricated by cosputtering deposi-tion with Sn nominal concentrations between 10 and 50 at% for amorphous (as-grown) samples and 10 and 60 at% for

Table 1. Sn concentration measured by EDX (relative to the total Ir + Sn) and cell parameters calculated by XRD and Rietveld refinements. Pure IrO$_2$ and SnO$_2$ thin films were also measured as references.

Sample	Sn concentration [%] ±2%	$a = b$ [Å]	c [Å]	Volume cell [Å^3]
IrO$_2$	0	4.484(2)	3.133(2)	63.0(1)
Ir$_{0.9}$Sn$_{0.1}$O$_2$	9	4.495(2)	3.142(2)	63.5(1)
Ir$_{0.8}$Sn$_{0.2}$O$_2$	19	4.510(4)	3.149(4)	64.1(1)
Ir$_{0.7}$Sn$_{0.3}$O$_2$	26	4.547(9)	3.151(9)	65.2(3)
Ir$_{0.6}$Sn$_{0.4}$O$_2$	42	4.590(4)	3.148(3)	66.3(1)
Ir$_{0.5}$Sn$_{0.5}$O$_2$	46	4.583(6)	3.176(6)	66.7(2)
Ir$_{0.4}$Sn$_{0.6}$O$_2$	63	4.605(4)	3.171(3)	67.2(1)
SnO$_2$	100	4.736(1)	3.185(1)	71.4(1)

polycrystalline (annealed) samples. Pure IrO$_2$ and SnO$_2$ thin films were also deposited with the same sputtering configuration to be used as reference materials. **Table 1** shows the Sn atomic percentages obtained from the energy-dispersive X-ray spectroscopy (EDX) analyses, which are found to be close to the nominal values. The cell parameters calculated by Rietveld refining the diffractograms shown in **Figure 1**a are also included. All the annealed films exhibit a polycrystalline non-textured microstructure whose Bragg peaks positions progressively shift from an IrO$_2$-like structure to a SnO$_2$-like structure as the Sn concentration is increased. Even though the peaks width is relatively large, which hinders a more precise analysis of the cell parameters, a nearly linear increase of the volume cell with the Sn content is obtained, as shown in Table 1 and Figure 1b.

Normalized high energy resolution fluorescence detected X-ray absorption near edge structure (HERFD-XANES) spectra were recorded at the Ir L$_{2,3}$-edges for the end members of the crystalline and amorphous series. **Figure 2**a compares the polycrystalline Ir$_{0.4}$Sn$_{0.6}$O$_2$ and IrO$_2$ samples, and Figure 2b the amorphous Ir$_{0.5}$Sn$_{0.5}$O$_2$ and IrO$_2$ samples. In all the cases, the HERFD-XANES data show strong "white lines" at both absorption edges, indicative of a large local density of 5d states.[14] Furthermore, at first glance, very similar spectral profiles can be observed regardless of the Sn amount, revealing very similar electronic structure and SOC for Sn-doped and pure IrO$_2$ samples. The branching ratio, defined as $BR = I_{L3}/I_{L2}$, where $I_{L2,3}$

is the integrated white line intensity at a particular spin–orbit split edge, is close to 4 for all the samples. These experimental values, approximately two times larger than the statistical $BR = 2$, imply the presence of large and robust SOC in all the cases.[15,16]

Looking carefully at the SOC values, more specifically the ground-state expectation value of the angular part of the SOC, $\langle L \cdot S \rangle$, calculated via $BR = (2+\langle L \cdot S \rangle/n)/(1-\langle L \cdot S \rangle/n)$, where n is the number of holes (see Figure 2c); it is very striking the higher SOC measured in the amorphous samples compared to those of the polycrystalline samples. As far as the Sn-doping is concerned, not only does the SOC not get worse, but it seems to increase. The value calculated for the Ir$_{0.5}$Sn$_{0.5}$O$_2$ amorphous sample is around 2% higher than for the amorphous IrO$_2$ thin film. The same tendency, even more evident, is observed in the polycrystalline samples. Here, the SOC is ≈10% higher in the doped film than in the pure IrO$_2$.

In order to understand the differences observed in the SOC depending on the microstructure, Figure 2d shows a comparison between the absorption spectra for both the amorphous and the polycrystalline IrO$_2$ samples. The amorphous samples present comparatively smaller white lines at both edges and a slight shift towards lower energies relative to the polycrystalline samples (≈0.3 eV). One could tentatively associate this shift to the presence of metallic Ir. However, as shown by Clancy et al.,[15] this would be translated into a reduction of the SOC. On the other hand, such energy shift could also be associated to larger Ir—O distances.[17–19] Unfortunately, no value of these distances can be inferred from X-ray diffraction (XRD) in amorphous samples.

Regarding the Sn-doping, the small SOC increment can also be associated with structural changes. In this case, the small shift (≤0.1 eV) toward lower energies observed in the doped samples relative to the IrO$_2$ samples can be hardly seen in the comparison displayed in the HERFD-XANES in Figure 2a,b. Nevertheless, according to XRD (see Figure 1), Sn atoms placed in Ir sites enlarge the volume cell toward the typical values of a SnO$_2$ lattice. This is likely to make the Ir—O distances larger, reducing the band overlap and increasing the SOC. Assuming a homogeneous volume expansion, a ≈1.8% increase, or in other words a ≈0.04 Å increase, in the Ir—O distance can be roughly estimated from our XRD data. This is a very small change that can be hardly detected by XAS, but it might be related to such SOC increase.
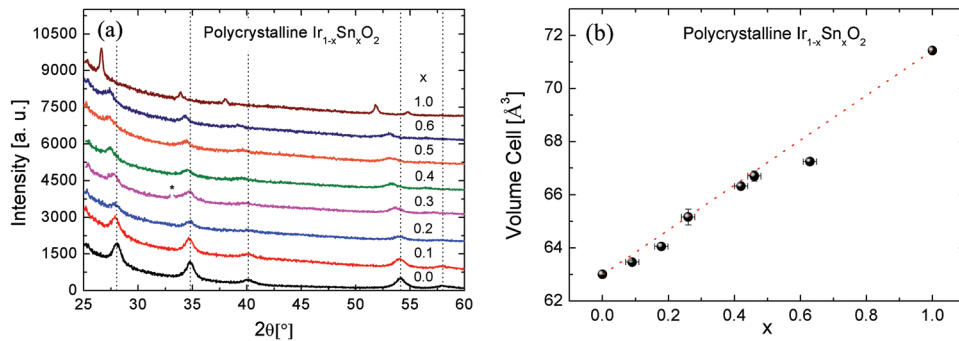

Figure 1. a) XRD profiles for annealed Ir$_{1-x}$Sn$_x$O$_2$ thin films. (*) substrate peak removed for clarity. b) Dependence of the volume cell with the Sn concentration (EDX) determined from the results of the Rietveld refinement. The dotted line is a guide for the eye.
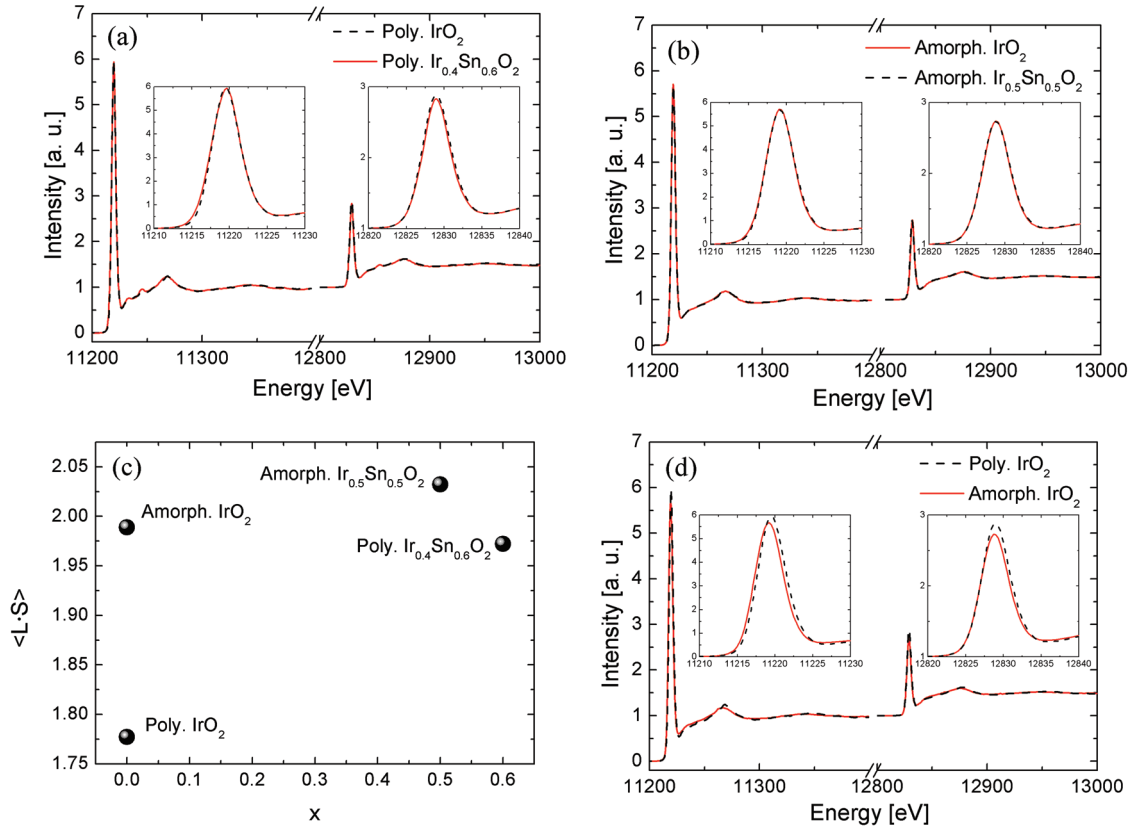
Figure 2. Representative comparisons between the normalized Ir $L_{2,3}$-edges HRFED-XANES spectra recorded on a) polycrystalline and b) amorphous pure and Sn-doped IrO_2 thin films. c) Plots the values of the SOC ($< L \cdot S >$ product) obtained from the XAS data. d) Compares the amorphous and polycrystalline states of pure IrO_2 samples.

Trying to shed further light on the role of the Ir—O distance on the SOC values, **Figure 3**a shows the Fourier transform (real part) of the k^2-weighted Ir L_3-edge extended X-ray absorption fine structure (EXAFS) signal. Here, it can be observed a small shift in the main peak at ≈1.65 Å (no phase correction applied) toward higher distances for amorphous and doped films. Figure 3b helps to see such evolution. The resemblance of this trend to that observed in Figure 2c points out that an

increase of the Ir—O bond distances is translated into higher SOC values.

Temperature-dependent electrical resistivity measurements, $\rho(T)$, from room temperature to 10 K are shown in **Figure 4**a,b for polycrystalline and amorphous $Ir_{1-x}Sn_xO_2$ samples, respectively.

First, the resistivity of the pure polycrystalline IrO_2 sample exhibits a metallic-like behavior (positive slope) in all the
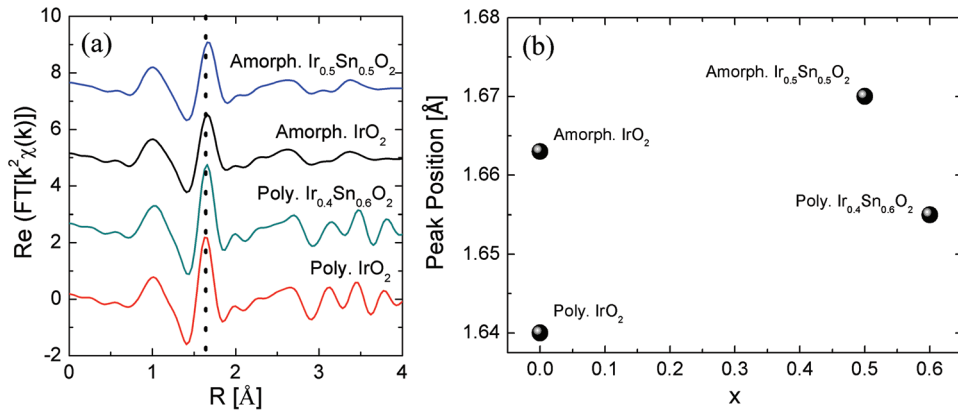

Figure 3. a) Fourier transforms (real part) of the k^2-weighted Ir L_3-edge EXAFS signal in the range from 3 Å^{-1} to 12 Å^{-1}. b) Evolution of the main-peak position.

temperature range measured, in accordance with previous results.[4,7–10] On the other hand, for the amorphous IrO_2 sample, a more complex behavior is observed. In the 300 to 250 K temperature range, it shows a semiconductor-like behavior (negative slope), since the resistivity rises slowly when decreasing the temperature. At around 250 K there is a maximum in the $\rho(T)$ curve, and then the resistivity starts to decrease in a metallic-like behavior. Nevertheless, the variations in resistivity with the temperature are very small, from 670 μΩ cm at room temperature to 690 μΩ cm at 10 K. Relative to the microstructure, the resistivity of the amorphous sample is found to be approximately four times larger than for the polycrystalline. As expected, the disorder of the amorphous samples hinders the conductive electrons in the film, increasing the electrical resistivity.

As Sn replaces Ir in the sample structure, there is an evident change in the slope of the $\rho(T)$ curves in the $x = 0.3$–0.4 range for the polycrystalline samples and in $x = 0.2$–0.3 for amorphous samples, turning from metallic-like into a semiconductor-like behavior. In addition, as shown in Figure 4cd for $T = 300$ K, there is an exponential dependence of the electrical resistivity with the Sn concentration for both the polycrystalline and amorphous state. For the polycrystalline samples, the resistivity at room temperature increases from 170 to 9250 μΩ cm, while in the amorphous samples the resistivity changes from 670 to 28 000 μΩ cm. The differences are even more evident at low temperature (10 K), where the resistivity increases almost

two orders of magnitude (from 130 to 10 500 μΩ cm) in the polycrystalline samples, and more than five orders of magnitude (from 690 to >10^8 μΩ cm, out of the PPMS range) for the amorphous samples. Note that for amorphous SnO_2, a resistivity of ≈2 × 10^7 μΩ cm was measured at room temperature and it went out of the PPMS range (>10^8 μΩ cm) when cooling below 155 K (not shown here). As the Sn^{4+} ions, with electronic configuration $[Kr]4d^{10}$, substitute the Ir^{4+} ions, $[Xe]\,4f^{14}5d^5$, the number of "barriers" for the conductive electrons progressively increases and so does the electrical resistivity. This indicates that by suitably choosing the Sn content it is possible to significantly tune the electrical response of the material.

3. Summary and Conclusions

IrO_2 has been proposed as the most promising material for spin current detection.[4] In order to explain and optimize the initial results observed by Fujiwara et al.,[4] we prepared for the first time Sn-doped IrO_2 thin films, $Ir_{1-x}Sn_xO_2$ ($x = 0$–0.6), by reactive magnetron cosputtering. The composition, structure, and electrical behavior have been analyzed by different techniques including XRD, EDX, XAS, HERFD-XANES, and electrical resistivity measurements. The films, in both the amorphous and the polycrystalline state, have been investigated and compared to pure IrO_2 thin films of approximately the same thickness.
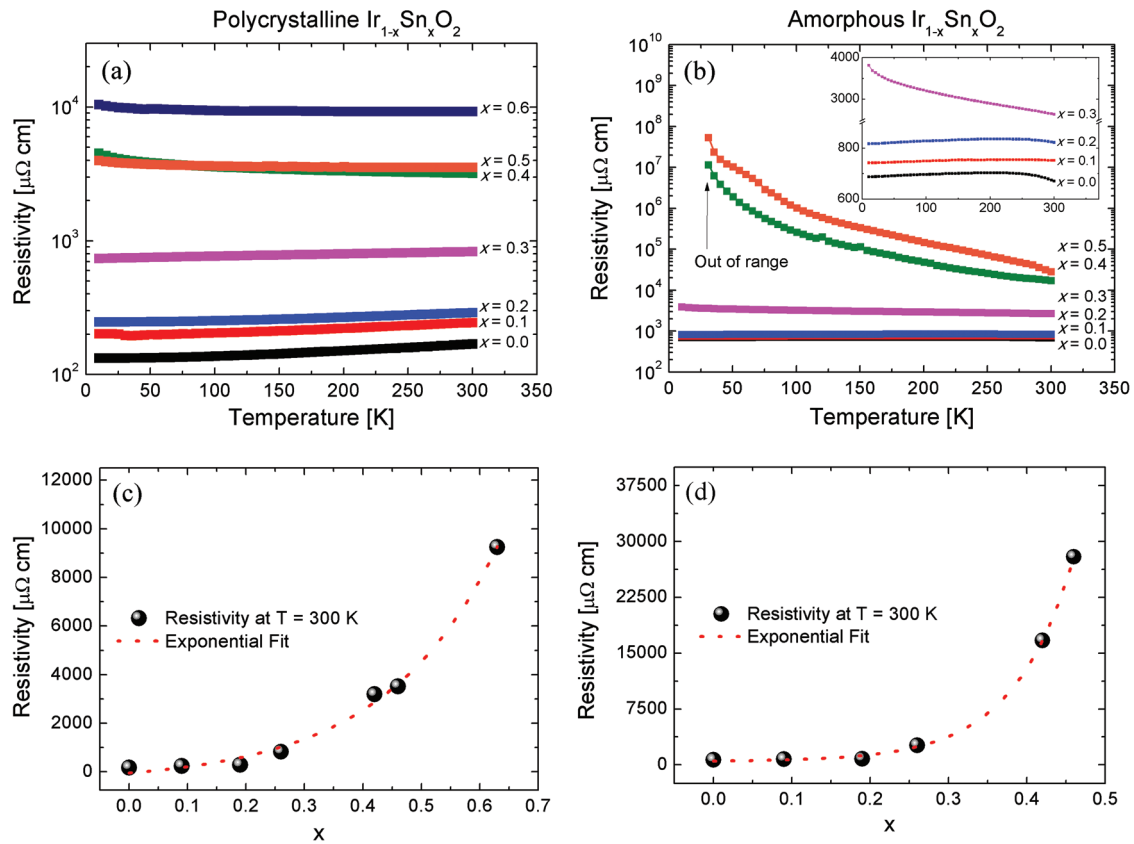

Figure 4. Electrical resistivity of a) polycrystalline, and b) amorphous $Ir_{1-x}Sn_xO_2$ thin films. The inset in panel b) allows seeing the details of samples with $x \le 0.3$. The evolution of the resistivity measured at 300 K is graphically plotted in panels c,d) for polycrystalline and amorphous samples, respectively.

The analysis of the HERFD-XANES data reveals very strong 5d SOC in all the samples. Moreover, the spin–orbit interaction is found to be slightly enhanced in the amorphous state, which would explain the results obtained by Fujiwara et al.[4] Similarly, the SOC slightly increases when doping IrO_2 with Sn atoms. From our XRD, HERFD-XANES, and EXAFS experiments, this SOC enhancement can be correlated, in both cases, to an increase on the Ir—O bond distances.

The electrical properties have been proved to be strongly dependent on the structural details. We have shown for the first time that by changing the Sn-doping and the microstructure of the IrO_2 thin films, its electrical resistivity can be tuned in a range of several orders of magnitude. Overall, our work prove that by growing $Ir_{1-x}Sn_xO_2$ films we can obtain samples with a large resistivity, up to at least five orders of magnitude larger than that on IrO_2 at 10 K, while keeping the system in a high and robust SOC regime. Consequently, it points to a clear new direction/approach in the quest of optimized materials for spin current detection.[5,6]

From the industrial application point of view, the good results obtained in the amorphous $Ir_{1-x}Sn_xO_2$ samples are especially relevant as they are easier to fabricate. Besides, taking into account the high price of Ir, Sn-doping also considerably reduces costs. Finally, shall we need better crystallized samples for better diffusion process at the interface, the crystalline $Ir_{1-x}Sn_xO_2$ films still present better SOC and resistivity response than the undoped IrO_2.

4. Experimental Section

Thin films were grown by cosputtering deposition configured with 2 in. Ir and SnO_2 targets, connected to DC and RF sources, respectively. The substrates, of ≈5 × 5 mm, were placed at a distance of 100 mm from the targets and the two magnetrons were tilted so that the substrate was located where their axes meet. Thus, homogeneous samples were obtained without rotating the substrate. The power supplied to the Ir target was settled at 8 W and the power supplied to the SnO_2 target was varied from 18 to 29 W in order to obtain different Sn concentrations. Within this power range, Sn nominal concentrations between 10 and 50 at% were probed. An O_2/Ar mixture gas ≈13% O_2 rich was used to grow all the samples. The base pressure provided by the vacuum system was in the 3–5 × 10^{-7} mbar range and the working pressure was ≈5 × 10^{-3} mbar. A ≈100 nm layer of the respective compound was first grown on Si(100) substrates at room temperature in order to study the amorphous state. The samples were subsequently annealed at 600 °C in air during 6 h to obtain polycrystalline samples. Additionally, one 50% Sn-doped sample was annealed at 900 °C. At this temperature, part of the Ir in the film reacts with the oxygen in air and it is evaporated as IrO_3.[8] This is how the 60% Sn-doped films were obtained. For simplicity purposes, samples are labeled as $Ir_{1-x}Sn_xO_2$, where x states for the nominal Sn concentration. Pure amorphous and polycrystalline IrO_2 thin films were also fabricated in the same chamber and properly characterized to use them as references.

The effects of different Sn concentration on both amorphous and polycrystalline films were investigated in terms of structural and electrical properties. First, X-ray reflectivity (XRR) and XRD measurements were performed on a BrukerD8 and on a Rigaku D/max 2500 X-ray diffractometers, respectively, by using the $K\alpha$ radiation line of copper. Sample thickness was checked by XRR (not shown here) and the cell parameters of the polycrystalline samples were calculated by Rietveld refining the XRD patterns using the Fullprof code.[20] The morphology and composition of the films were investigated under field-emission scanning electron microscope (FE-SEM) and EDX, respectively.

HERFD-XANES measurements were carried out at room temperature at beamline I20 scaning at diamond light source.[21,22] The beamline was equipped with a four-bounce scanning Si(111) monochromator,[23] and the harmonic rejection was achieved by using two Rh-coated mirrors operating at 4.0 mrad incidence angle. An X-ray emission spectrometer based on a 1 m diameter Rowland circle operating in the Johann configuration in the vertical plane was used for the experiment.[24] Three 100 mm Si(555) spherical analyzer crystals were used to select the $L_{\beta 1}$ (10 708 eV) emission line, while three 100 mm Si(642) crystals were used in the case of the $L_{\alpha 1}$ (9175 eV) emission line. An ion chamber filled with the optimum gas mixture to absorb 15% of the incident radiation at the Ir L_3 and L_2-edge energies was used as incident monitor, while a Medipix area detector[25] was used to collect the intensity of the emission line. HERFD-XANES enhances features present in the edge region of the absorption spectrum by reducing the core-hole lifetime,[26] thus resolving structures that are not visible in a conventional XANES spectrum.[27,28]

The strength of the SOC, more specifically the ground-state expectation value of the angular part of the SOC, $\langle L \cdot S \rangle$, was determined by applying sum rule analysis to the HERFD-XANES spectra.[16] The Ir—O bond distances were determined by analyzing the EXAFS region on the absorption spectra. Such spectra were collected at the CLAESS beamline at ALBA synchrotron. A Si(111) double crystal monochromator was used to obtain a monochromatic beam, and Rh-coated collimating and toroidal mirrors were used to optimize the energy resolution, to focus the beam and to reject higher harmonics.

Finally, the electrical resistivity was measured using the four points van der Pauw method[29] by means of a Quantum Design PPMS 9T from 300 to 10 K with no applied magnetic field and with a small electric current (0.1 mA).

Conflict of Interest

The authors declare no conflict of interest.

[1] T. Seki, Y. Hasegawa, S. Mitani, S. Takahashi, H. Imamura, S. Maekawa, J. Nitta, K. Takanashi, *Nat. Mater.* **2008**, *7*, 125.

[2] K. Ando, E. Saitoh, *J. Appl. Phys.* **2010**, *108*, 113925.

[3] M. Morota, Y. Niimi, K. Ohnishi, D. H. Wei, T. Tanaka, H. Kontani, T. Kimura, Y. Otani, *Phys. Rev. B* **2011**, *83*, 174405.

[4] K. Fujiwara, Y. Fukuma, J. Matsuno, H. Idzuchi, Y. Niimi, Y. Otani, H. Takagi, *Nat. Commun.* **2013**, *4*, 2893.

[5] K. Ando, E. Saitoh, *Nat. Commun.* **2012**, *3*, 629.

[6] L. Vila, T. Kimura, Y. Otani, *Phys. Rev. Lett.* **2007**, *99*, 226604.

[7] M. Uchida, W. Sano, K. S. Takahashi, T. Koretsune, Y. Kozuka, R. Arita, Y. Tokura, M. Kawasaki, *Phys. Rev. B* **2015**, *91*, 241119.

[8] Y. Liu, H. Masumoto, T. Goto, *Mater. Trans.* **2004**, *45*, 3023.

[9] R. H. Horng, D. S. Wuu, L. H. Wu, M. K. Lee, *Thin Solid Films* **2000**, *373*, 231.

[10] W. J. Kim, S. Y. Kim, C. H. Kim, C. H. Sohn, O. B. Korneta, S. C. Chae, T. W. Noh, *Phys. Rev. B* **2016**, *93*, 045104.

[11] B. Gu, I. Sugai, T. Ziman, G. Y. Guo, N. Nagaosa, T. Seki, K. Takanashi, S. Maekawa, *Phys. Rev. Lett.* **2010**, *105*, 216401.

[12] A. Fert, P. Levy, *Phys. Rev. Lett.* **2011**, *106*, 157208.

[13] M. Gradhand, D. V. Fedorov, P. Zahn, I. Mertig, Y. Otani, Y. Niimi, L. Vila, A. Fert, *SPIN* **2012**, *2*, 1250010.

[14] M. A. Laguna-Marco, D. Haskel, N. Souza-Neto, J. C. Lang, V. V. Krishnamurthy, S. Chikara, G. Cao, M. van Veenendaal, *Phys. Rev. Lett.* **2010**, *105*, 216407.

[15] J. P. Clancy, N. Chen, C. Y. Kim, W. F. Chen, K. W. Plumb, B. C. Jeon, T. W. Noh, Y. J. Kim, *Phys. Rev. B* **2012**, *86*, 195131.

[16] G. van der Laan, B. T. Thole, *Phys. Rev. Lett.* **1988**, *60*, 1977.

[17] J. Chaboy, *J. Synchrotron Radiat.* **2009**, *16*, 533.

[18] M. Tromp, J. Moulin, G. Reid, J. Evans, presented at *13th Int. Conf. X-ray Absorption Fine Structure*, Stanford, July **2006**.

[19] P. Glatzel, G. Smolentsev, G. Bunker, presented at *14th Int. Conf. X-ray Absorption Fine Structure*, Camerino, July **2009**.

[20] J. Rodriguez-Carvajal, *Phys. B* **1993**, *192*, 55.

[21] S. Diaz-Moreno, S. Hayama, M. Amboage, A. Freeman, J. Sutter, G. Duller, presented at *14th Int. Conf. X-ray Absorption Fine Structure*, Camerino, July **2009**.

[22] S. Diaz-Moreno, M. Amboage, M. Basham, R. Boada, N. E. Bricknell, G. Cibin, T. M. Cobb, J. Filik, A. Freeman, K. Geraki, D. Gianolio, S. Hayama, K. Ignatyev, L. Keenan, I. Mikulska, J. F. W. Mosselmans, J. J. Mudd, S. A. Parry, *J. Synchrotron Radiat.* **2018**, *25*, 998.

[23] S. Hayama, G. Duller, J. P. Sutter, M. Amboage, R. Boada, A. Freeman, L. Keenan, B. Nutter, L. Cahill, P. Leicester, B. Kemp, N. Rubies, S. Diaz-Moreno, *J. Synchrotron Radiat.* **2018**, *25*, 1556.

[24] H. H. Johann, *Z. Phys.* **1931**, *69*, 185.

[25] R. Plackett, I. Horswell, E. N. Gimenez, J. Marchal, D. Omar, N. Tartoni, *J. Instrum.* **2013**, *8*, C01038.

[26] K. Hamalainen, D. P. Siddons, J. B. Hastings, L. E. Berman, *Phys. Rev. Lett.* **1991**, *67*, 2850.

[27] F. M. F de Groot, M. H. Krisch, J. Vogel, *Top. Catal.* **2000**, *10*, 179.

[28] P. Glatzel, U. Bergmann, *Coord. Chem. Rev.* **2005**, *249*, 65.

[29] L. J. van der Pauw, *Philips Res. Rep.* **1958**, *13*, 1.